Geofísica Internacional (2017) 56-3: 269-286

Original paper

Observations of remotely triggered seismicity in Salton Sea and Coso geothermal regions, Southern California, USA, after big (MW>7.8) teleseismic earthquakes

Raúl R. Castro*, Robert Clayton, Egill Hauksson and Joann Stock

Received: September 27, 2016; accepted: January 08, 2017; published on line: July 01, 2017

Resumen

Se analizó un catálogo de sismos relocalizados en las regiones cercanas a los campos geotérmicos de Coso y Salton Sea, en el sur de California, USA, para investigar posibles cambios en la tasa de sismicidad durante y después de telesismos grandes (*Mw*>7.8). Se estudió la sismicidad de estas dos regiones usando ventanas de 30 días previos y posteriores a la ocurrencia de cinco grandes sismos: el de Denali, Alaska del 2002 (*Mw*7.9); el de Sumatra-Andaman del 2004 (*Mw*9.2); el de Chile del 2010 (*Mw*8.8); el de Tohoku-Oki, Japón del 2011 (*Mw*9.1); y el del norte de Sumatra del 2012 (*Mw*8.6).

El sismo de Denali (*Mw*7.9) coincide con un incremento de la sismicidad en la región del Salton Sea cuando este evento remoto ocurrió, indicando que el disparo instantáneo de la sismicidad está posiblemente relacionado con el paso de las ondas superficiales en esta región. En la región del campo geotérmico Coso la tasa de sismicidad permaneció aproximadamente constante durante el periodo de 30 días de observación. La sismicidad después del sismo de Sumatra-Andaman del 2004 (*Mw*9.2) incrementó en las dos regiones 9 días después de este mega-evento. La sismicidad después del sismo de Chile del 2010 (*Mw*8.8) incrementó en ambas regiones aproximadamente 14 días después de la ocurrencia de este telesimo. La sismicidad en las regiones de Salton Sea y de Coso incrementaron 17 y 14 días, respectivamente, después del terremoto de Japón del 2011 (*Mw*9.1), lo que sugiere que el disparo retrasado de la sismicidad fue inducido después del paso de las ondas superficiales en ambas regiones. De manera similar el sismo del norte de Sumatra del 2012 (*Mw*8.6) disparó sismicidad 6 y 16 días después en las regiones de Salton Sea y Coso, respectivamente. Estas observaciones se pueden interpretar como evidencia de disparo dinámico retrasado inducido por sismos grandes y remotos. Encontramos que la magnitud máxima de los enjambres sísmicos disparados incrementa con el tamaño (M_0/Δ) de los mega-sismos y que cuando el tamaño de estos se incrementa, el tiempo de retraso también aumenta.

Palabras clave: disparo remoto, sismicidad del sur de California, USA, campo geotérmico Coso, campo geotérmico Salton Sea.

R. R. Castro*
CICESE
Departamento de Sismología
Ensenada, Baja California
México,
**Corresponding author: raul@cicese.mx*

R. Clayton
E. Hauksson
J. Stock
CALTECH
Seismological Laboratory
Pasadena, California, USA

Abstract

A relocated catalog was used to search for changes in seismicity rate in the Salton Sea and the Coso geothermal regions, southern California, USA, during and after large (M_w>7.8) teleseismic earthquakes. Seismicity in these two regions was analyzed within 30-day windows before and after the occurrence of five major earthquakes: the 2002 Denali fault, Alaska (M_w7.9); the 2004 Sumatra-Andaman (M_w9.2); the 2010 Central Chile (M_w8.8); the 2011 Tohoku-Oki, Japan (M_w9.1); and the 2012 Offshore Northern Sumatra (*Mw*8.6) earthquakes.
The Denali (M_w7.9) earthquake coincided with an increase in seismicity in the Salton Sea region the day when this remote event occurred, indicating that instantaneous triggered seismicity was likely related with the passage of its surface waves. However, in the Coso region the seismicity rate remained approximately constant during the 30-day observation period. The seismicity after the 2004 Sumatra-Andaman (M_w9.2) earthquake increased in both regions 9 days after the mega-earthquake. The seismicity after the 2010 Chile (M_w8.8) earthquake increased in both regions approximately 14 days after the remote event. The seismicity in Salton Sea and Coso regions increased 17 and 14 days, respectively, after the 2011 Japan (M_w9.1) earthquake, suggesting that delayed triggered seismicity was induced after the passage of the surface waves in both regions. Similarly, 6 and 16 days after the 2012 northern Sumatra (M_w8.6) earthquake the seismicity also increased in Salton Sea and Coso regions, respectively. These observations can be interpreted as evidence of instantaneous and delayed dynamic triggering induced by large remote earthquakes. The maximum magnitude of the delayed triggered swarm increased with the strength (M_0/Δ) of the mega-earthquake and, the stronger the remote earthquake, the longer the delay time.

Key words: remote triggering, seismicity southern California, USA, Coso geothermal field, Salton Sea geothermal field.

Introduction

Since the 1992, M_w7.3 Landers earthquake, several studies have documented that large distant earthquakes can dynamically trigger seismicity (Hill *et al*., 1993; Anderson *et al*. 1994; Gomberg and Bodin, 1994; Hill and Prejean, 2007; Peng and Gomberg, 2010), particularly in volcanic and geothermal regions. Velasco *et al*. (2008) and Jiang *et al*. (2010) showed that the dynamic stress generated by both Rayleigh and Love waves can increase significantly the crustal stress in active regions, which can trigger micro-earthquakes. Based on the analysis of dynamic stress associated with the fundamental mode of Rayleigh and Love waves (Hill, 2008), the triggering potential of the surface waves was defined by Gonzalez-Huizar and Velasco (2011) as the change of the Coulomb failure function caused by the passage of the seismic wave. The triggering potential depends also on the faulting mechanism that is being triggered. The physical processes of dynamic triggering have been related with geothermal activity, including magma intrusions, movement of magmatic fluids and bubble excitation (Hill *et al*., 1993; Linde and Sacks, 1998). Long-period waves that generate fluid flow can lead to high-pressure oscillations (Brodsky and Prejean, 2005) and likely temporal variations of seismicity.

Withdrawal and injection of fluids can also change pore pressure and modify normal stress driving local faults to failure (Hubbert and Rubey, 1959). Seismicity induced in geothermal fields has been analyzed in Coso (Feng and Lees, 1998) and Salton Sea (Brodsky and Lajoie, 2013) regions, USA. More recently Trugman *et al*. (2016) studied long-term changes in seismicity at these two regions and found that the seismicity rate in both of them correlates with fluid withdrawal and injection only before 1990, during the beginning of the geothermal field operations.

In the present study, temporal variations of local seismicity are analyzed in two geothermal related regions, the Coso Range and the Salton Sea, before and after the occurrence of five major earthquakes: the 2002 Denali fault, Alaska (M_w7.9); the 2004 Banda Ache, Sumatra-Andaman (M_w9.2); the 2010 Central Chile (M_w8.8); the 2011 Tohoku-Oki, Japan (M_w9.1); and the 2012 northern Sumatra (*Mw*8.6) earthquakes. In particular, the time delay between the origin time of large remote earthquakes and the triggered seismicity variation with the strength (M_0/Δ) of the teleseismic events and these with the maximum magnitude of the triggered earthquake swarm are analyzed.

Tectonic framework

The Coso Geothermal Region

The Coso geothermal field is located in a releasing bend in a right-lateral fault system west of Death Valley, north of the Mojave Desert and east of southern Owens valley (Monastero *et al*., 2005). The location of the Coso range, the main topographic features of the region and the seismicity analyzed are displayed in the map of Figure 1. The Coso Geothermal Field (CGF) is located in the central zone of the Range and is one of the most seismically active regions in central California, USA (Bhattacharyya and Lees, 2002). The Coso Range has a high level of seismicity, resulting from dextral transtension along the eastern margin of the Sierra Nevada microplate and other processes related to the CGF. Moderate size earthquakes have occurred in this region in the past, for instance, from 1981 to 2005 several events with $M \leq 5.8$ were reported by Hauksson *et al*. (1995) near Ridgecrest. Remotely triggered seismicity has been reported previously at Coso after the 1992 Landers earthquake (Hill *et al*., 1993), and by other large teleseismic earthquakes like the 2002 Denali fault earthquake (Prejean *et al*., 2004). Aiken and Peng (2014) analyzed local earthquakes triggered by distant earthquakes with magnitudes greater than 5.5 that occurred in the Coso Geothermal Field between 2000 and 2012. They found that the triggering frequency of local earthquakes in Coso varied 3.8% in the 12 year period analyzed, and that the stress triggering threshold is approximately 1 KPa in this region.

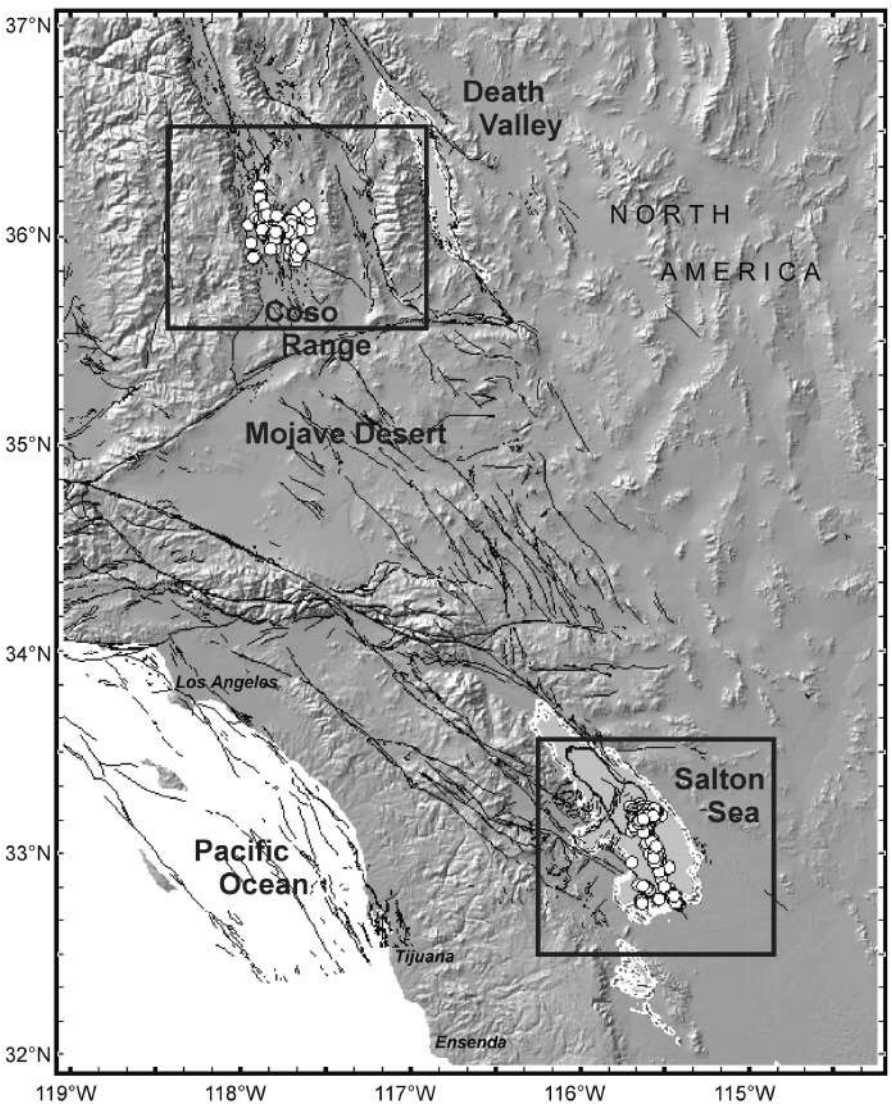

Figure 1. Location of regions studied (Coso and Salton Sea) and seismicity taken from the Hauksson-Yang-Shearer Alternative catalog of Southern California. The topography and bathymetry are from GeoMap App (Ryan *et al*., 2009). The boxes delimit the two regions of interest shown in Figures 2 and 3.

Salton Sea

Oblique extension in this region of southern California originated the Salton Trough, a topographic depression (endorheic basin) that links the San Andreas Fault system to the Gulf of California rift system (Elders *et al*., 1972; Stock and Hodges, 1989). The basin includes the Coachella, Imperial, and Mexicali Valleys, and contains the sub-sea-level Salton Sea in the central depression. Main transform faults of the depression included the Imperial fault, the Cerro Prieto Fault, and the southern San Andreas Fault. The Salton Sea Geothermal Field is located in the extensional step-over between the San Andreas and Imperial faults (Muffler and White, 1969). Earthquake swarms are generated frequently in the spreading centers south of Salton Sea but the largest earthquakes occur on the main transform faults (Doser and Kanamori, 1986; Hauksson, 2011). The underlying crust consists of sediments and new oceanic crust (Fuis *et al*., 1984; Barak *et al*., 2015), with higher heat flow than in the neighboring ranges (Lachenbruch *et al*., 1985). The sediments of the Imperial Valley have a thickness of 5-6 km grading into metamorphic rocks (Fuis *et al*., 1984; Barak *et al*., 2015). The Salton Sea Basin and the Laguna Salada Basin, the regions with the lowest elevation in the Salton Trough, have the lowest upper mantle velocities, suggesting a connection between rift-related subsidence and deep magmatic activity (Barak *et al*., 2015). Previous studies in this region (Hough and Kanamori, 2002; Doran *et al*., 2011) have observed remote triggering of seismicity.

Data and method

Previous studies of triggered seismicity in southern California (e.g. Prejean *et al*., 2004) have used the standard Southern California Seismic Network (SCSN) earthquake catalog. We used the 2011-Hauksson-Yang-Shearer alternative catalog for Southern California (Hauksson *et al*., 2012; Lin *et al*., 2007) to analyze temporal changes of seismicity after the occurrence of the five mega earthquakes mentioned above. This catalog contains hypocentral coordinates relocated from the SCSN data base from 1981 and recently updated to 2014. Quarry blasts have been removed from this alternative catalog. The relocation procedure accounts for local variations in the velocity structure by applying various techniques in post-processing of the data. The absolute picks combined with the differential travel times are applied to improve the relative locations within clusters of similar events. Trugman *et al*. (2016) estimated the minimum magnitude of completion of this catalog and found that for the years 1981-2013 the catalog is complete above magnitude 2.0 for Salton Sea and above 1.5 for Coso.

From the alternative catalog events that occurred between October 2002 and May 2012 in the Coso region (35.87N-36.25N and 117.5W-118.0W) and in the Salton Sea region (32.75N-33.25N and 115.25W-115.70W) (Figure 1) were selected to analyze temporal seismicity variations for 30-day periods before and after the five big teleseismic events.

For the Coso region only shallow events (focal depth less or equal to 3 km)were selected for the analyses because these events are more likely related to the geothermal activity in this region. Approximately 60% of the events reported by the SCSN catalog have focal depths less than 3 km in the Coso Range and 30% have depths between 3 and 6 km. The rest of the events (~10%) have focal depths between 6 and 12 km. Hauksson and Unruh (2007) found localized low *P*- and *S*-wave velocity zones beneath the central Coso Range at 0-3 km depth that image the geothermal reservoir.

The local earthquakes that occurred in the Coso region in the 30 day periods before each of the remote earthquakes are displayed with light dots in Figure 2 and with dark dots the local events that occurred in the subsequent 30 days. The seismicity after the remote earthquakes (dark dots) seems to follow the same distribution pattern as the pre-event seismicity, suggesting that the seismicity triggered zones were already active. Similarly, Figure 3 shows the location of the earthquakes in the Salton Sea region for the 30-day periods before and after the remote earthquakes. The seismicity that presumably triggered after the passage of surface waves (dark dots) tends to concentrate near the Salton Sea geothermal field, located in the north of the studied area. In particular, before the 2012 Offshore Northern Sumatra M_w8.6 earthquake, the seismicity near the Salton Sea (light dots in Figure 3e) was distributed along the Imperial fault and in the Brawley seismic zone on a conjugate-fault trending NE-SW. Then, after the remote event most of the local earthquakes concentrated along the NE-SW direction, in the Salton Buttes area (site of Holocene volcanism; Schmitt *et al*., 2013) presumably in a small spreading center. This suggests that the tectonic stress had been concentrating in that zone before the mega-earthquake and that the dynamic stress increased the existing stress enough to trigger the seismicity where more stress had accumulated.

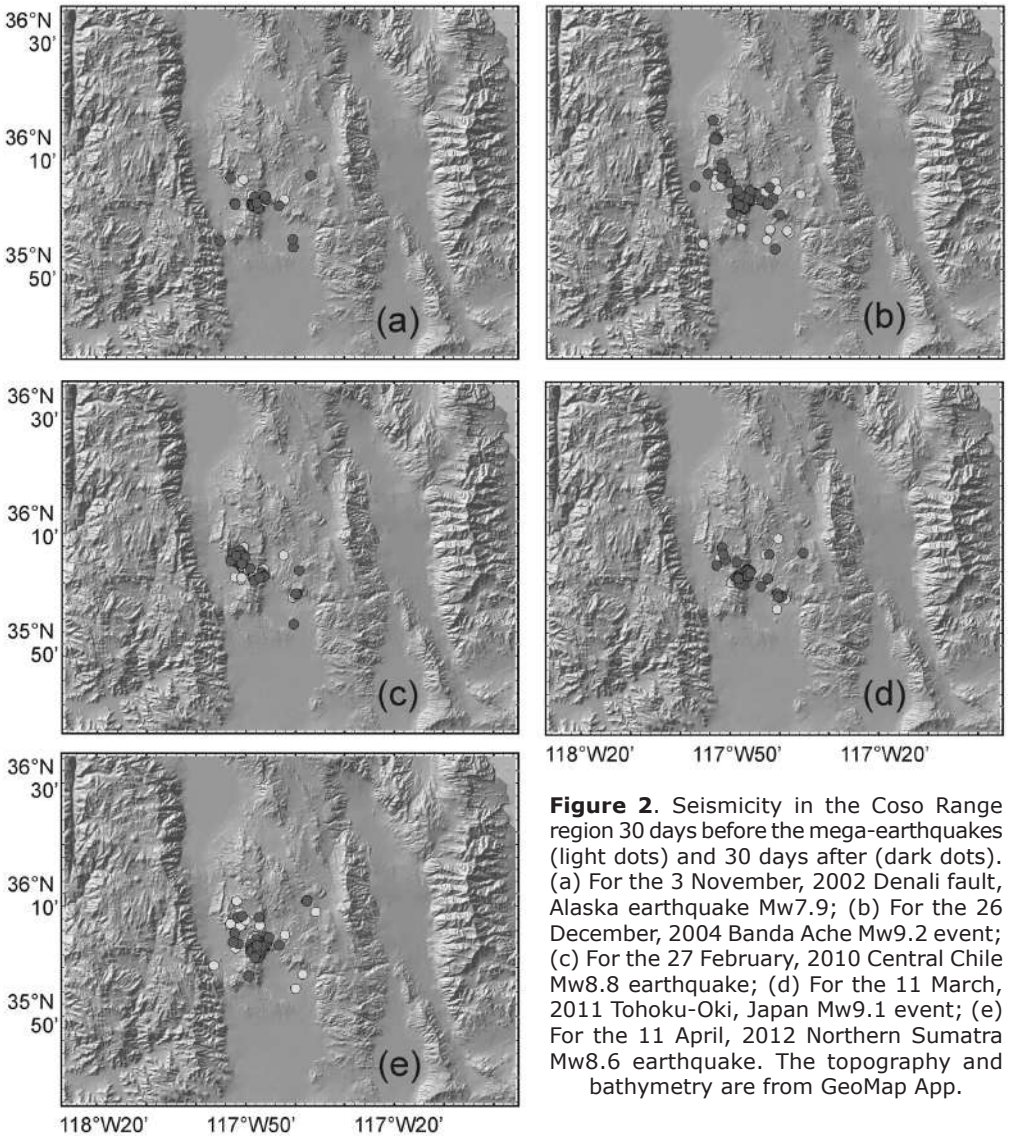

Figure 2. Seismicity in the Coso Range region 30 days before the mega-earthquakes (light dots) and 30 days after (dark dots). (a) For the 3 November, 2002 Denali fault, Alaska earthquake Mw7.9; (b) For the 26 December, 2004 Banda Ache Mw9.2 event; (c) For the 27 February, 2010 Central Chile Mw8.8 earthquake; (d) For the 11 March, 2011 Tohoku-Oki, Japan Mw9.1 event; (e) For the 11 April, 2012 Northern Sumatra Mw8.6 earthquake. The topography and bathymetry are from GeoMap App.

To quantify the statistical significance of seismicity rate changes, we compute β-statistics. This statistical parameter has been used before (e.g. Aron and Hardebeck, 2009) to compare the difference between the number of events occurring in a given time period and the expected number of events in that time period for a constant seismicity rate, normalized by the standard deviation (Matthews and Reasenberg, 1988).

The β-statistic is defined as:

$$\beta = \frac{N_i - NT_i / T}{N \frac{T_i}{T} \left(1 - \frac{T_i}{T}\right)^{1/2}} \qquad (1)$$

where T_i is the duration of the time period of interest and T is the duration of the whole catalog. N_i and N are the number of events in the time period of interest and the total number of events, respectively. For $|\beta| \geq 1.64$, the difference in seismicity rate between the two time periods is significant at 90% confidence; for $|\beta| \geq 1.96$, it is at 95% confidence, and for $|\beta| \geq 2.57$, it is significant at 99% confidence.

Data sets: triggered seismicity

The number of local events per day that occurred within a 30-day period before and after the remote mega-earthquakes selected is displayed in Figures 4 and 5 for the Coso Range and the Salton Sea regions, respectively. These figures illustrate the temporal variability of the seismicity rate. Time zero corresponds to the day when the remote earthquake occurred.

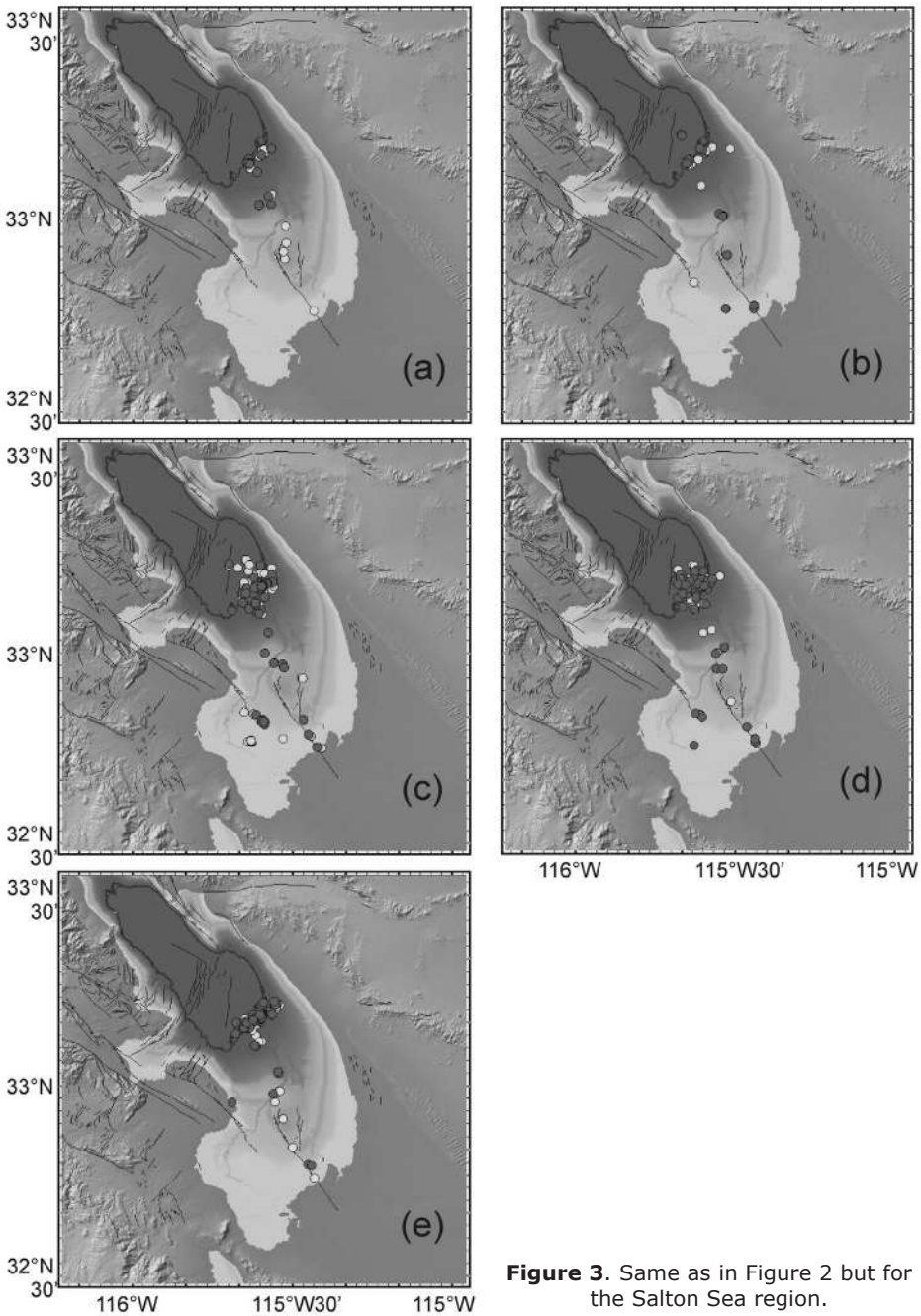

Figure 3. Same as in Figure 2 but for the Salton Sea region.

The Denali fault Mw7.9 earthquake

Remotely triggered seismicity following this earthquake has been extensively studied (Eberhart-Phillips *et al*., 2003; Gomberg *et al*., 2004; Pankow *et al*., 2004; Prejean *et al*., 2004; Hough, 2007; Jiang *et al*., 2010; Peng *et al*., 2011). The CGF is approximately 3700 km south east of the Denali fault epicenter and in general the Coso region does not show a significant increase in number of events until 26 days after the Denali earthquake (Figure 4, top). Aiken and Peng (2014) found events that triggered by the Denali earthquake by analyzing waveforms from a local station. They also found that most micro-earthquakes triggered were not detected by earthquake catalogs like ANSS because the low magnitude of these events (M<2). We detected only two events in the alternative catalog for Southern California (Figure 4) on 3 November 2002, the origin date of the Denali earthquake. The peak dynamic stress estimated by Prejean *et al*. (2004) from Love waves is ~0.01 MPa

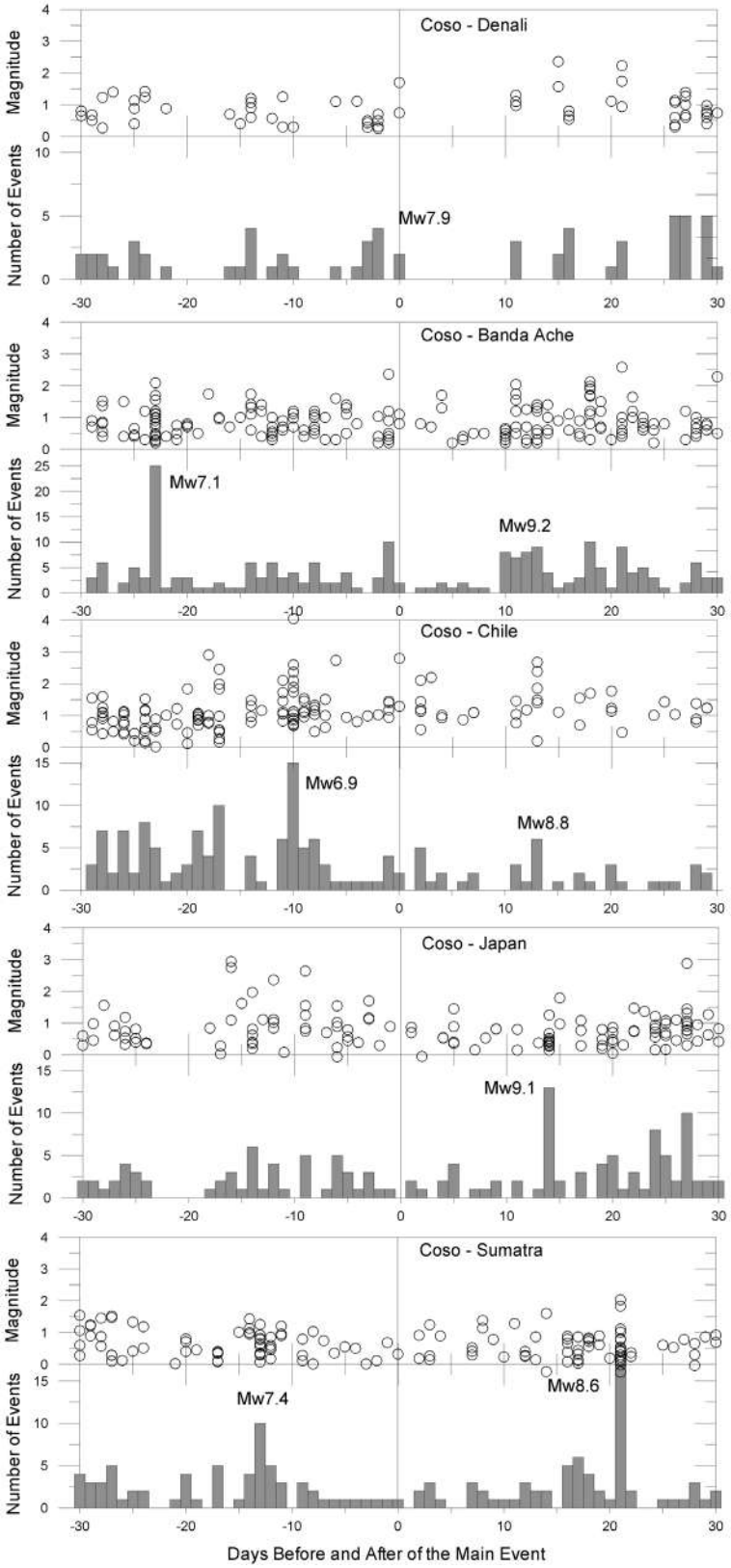

Figure 4. Number of events within a 30-day period before and after the remote big earthquakes in the Coso region and magnitudes of the triggered event. The numbers close to the peaks indicate the magnitude of the teleseism associated to the seismicity increase.

and ~0.03 MPa from Rayleigh wave arrivals, and the magnitude of the largest triggered earthquake was *M*=2.3. They also observed that the seismicity rate in Coso did not change significantly, based on the beta statistic on the SCSN catalog.

In the Salton Sea region (Figure 5, top) the seismicity increased significantly the same day of the 2002 Denali earthquake, indicating instantaneous triggering during the passage of the surface waves. The largest event triggered has a magnitude *M*=3.25 and smaller events occurred 14 days after with magnitudes between 1.4 and 2.2.

The Banda Ache, Sumatra-Andaman Mw9.2 earthquake

Dynamic triggering following this mega-earthquake has been studied by West *et al*. (2005) and Velasco *et al*. (2008). The local earthquakes at Mount Wrangell, Alaska occurred at depths of 2 km or less with magnitudes up to 1.9. Rayleigh waves produced vertical trough-to-peak ground motion displacements of 1.5 cm and generated stresses that reached 25 kilopascals.

The seismicity increased in the Coso and Salton Sea regions 9 days after the mega-earthquake. It is notable in Figures 4 (second row) the seismicity peak 24 days before the *Mw*9.2 event. We searched in the International Seismological Centre (ISC) catalog for large teleseismic events that could correlate with that seismicity peak and found a *M*7.1 earthquake that occurred in Papua at a depth of 10 km, on November 11, 2004, 21 days before the seismicity peak in the Coso region. In the Salton Sea region the seismicity also increased before the *Mw*9.2 Banda Ache, Sumatra earthquake (21 days before) and 24 days after the *M*7.1 Papua earthquake.

The Central Chile Mw8.8 earthquake

This event triggered seismicity in both regions 13-14 days after this mega-earthquake (Figures 4 and 5, third row). There were also increases in seismicity 10 and 5 days before the Chile earthquake in Coso and Salton Sea, respectively. That seismicity peak at the Salton Sea could have been induced by a *M*6.9 teleseismic earthquake located in the China-Russia-North Korea border at a depth of 25 km, on February 18, 2010. The seismicity peak in the Coso area may be related to the regional seismic activity. Remote triggered seismicity in the Coso Range following the 2010 Central Chile M_w8.8 earthquake has been studied in detail by Peng *et al*. (2010). They observed that the largest earthquake triggered (M_L3.5) occurred during the passage of the Love-wave peak amplitude. The Chile M_w8.8 earthquake also triggered seismicity in the El Mayor-Cucapah fault, Baja California region, Mexico, where the seismicity increased 10-20 days after this earthquake (Castro *et al*., 2015).

The 2011 Tohoku-Oki, Japan Mw9.1 earthquake

The M_w9.1 Japan earthquake generated large surface waves that impacted local seismicity thousands of kilometers away from the source region. Gonzalez-Huizar *et al*. (2012) identified several regions in the United States, Russia, China, Ecuador and Mexico where seismicity was triggered during and after the passage of the surface waves.

The 2011 Tohoku-Oki mega-earthquake presumably induced delayed seismicity 14 and 17 days after the origin time in the Coso and Salton Sea regions, respectively (Figures 4 and 5, fourth row). In the Salton Sea area there are also seismicity peaks the same day of the Japan mega-event and 5 days before, suggesting that instantaneous triggering also occurred in this region. The seismicity peak observed 5 days before may be related to the *M*6.5 South Sandwich Islands earthquake that occurred on March 6, 2011, the same day of the seismicity peak in the Salton Sea region.

The 2012 Offshore Northern Sumatra Mw8.6 earthquake

The Indian Ocean M_w8.6 earthquake is the largest strike-slip event ever recorded (Pollitz *et al*., 2012) and caused strong shaking in Indonesia, Japan and in the Gulf of California, Mexico. Several *M*>5.5 events were delayed triggered worldwide, unlike those in previous remote-triggering cases. Aiken and Peng (2014) found that this earthquake did not trigger instantaneously microearthquakes at Coso during the arrival of surface waves.

Within the 30-day period after the 2012 Sumatra earthquake the seismicity increased on days 16 and 6 in the Coso and Salton Sea regions, respectively (Figure 4 and 5, fifth row). There is a prominent peak 12 and 19 days before this remote event in the Coso and Salton Sea, respectively, that could be related to the *M*7.4 Oaxaca, Mexico, earthquake of March 20, 2012.

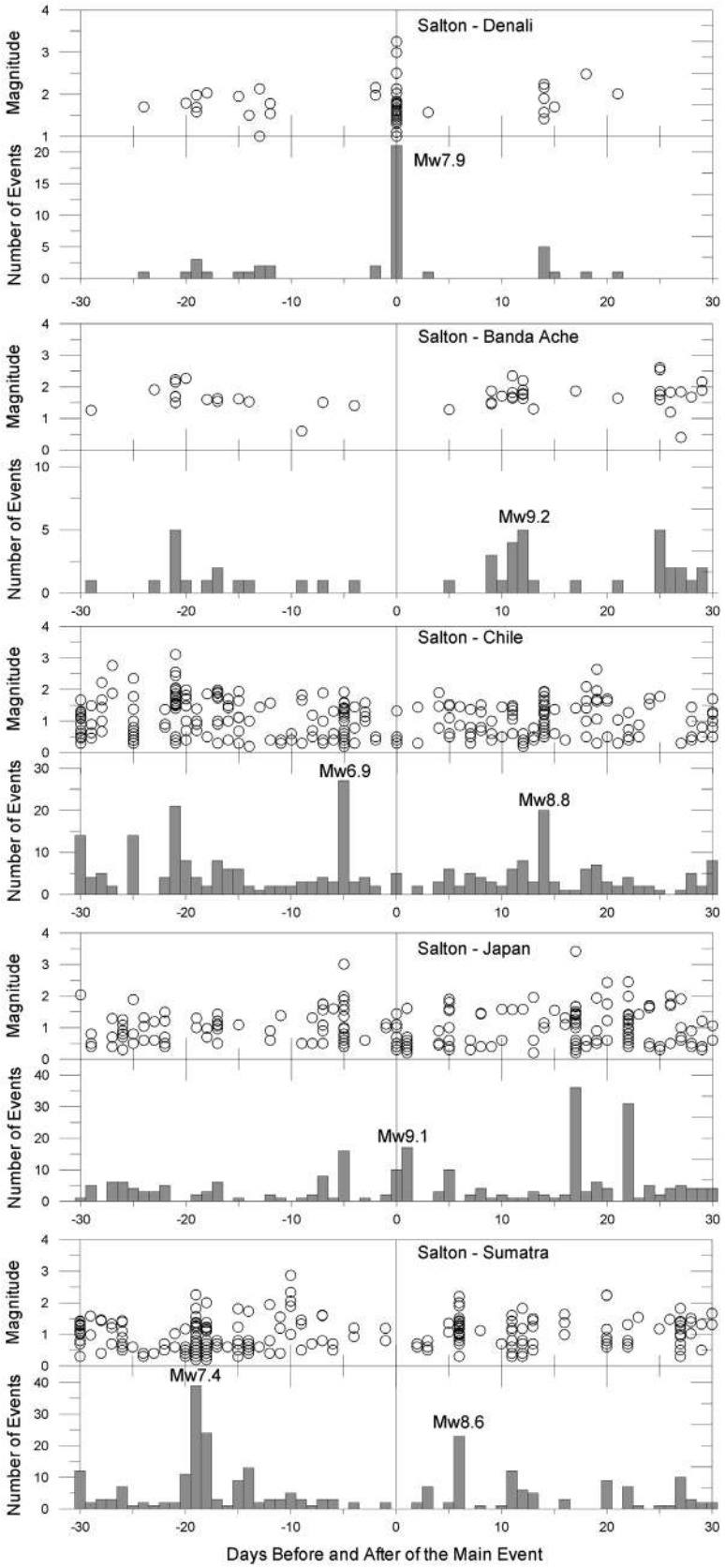

Figure 5. Same as in figure 4 but for the Salton Sea region.

Results

We analyzed longer seismicity time intervals to have a better perspective on the possible influence of other large remote earthquakes on the variability of seismicity rates observed in the Salton Sea region. In Figure 6 we show the number of events per day for a 6-month period before and after the 2002 Denali M_w7.9 and the 2004 Banda Ache M_w9.2 earthquakes. We focus on these two events because the first one shows a clear instantaneous triggering signal in the Salton Sea region and the second is the largest of the five mega-earthquakes analyzed. The vertical lines in Figure 6 indicate the day when a big (M>7.0) and remote earthquake occurred worldwide. During 2002 there were 12 big teleseismic events and 17 during 2004, and the seismicity in the Salton Sea region varied from 426 events in 2002 to 407 local events in 2004. In 2002 there was a seismicity peak on day 295 that cannot be associated to any M>7 remote event but there was a M6.6 earthquake at 19 km depth in Unimak Island region, Alaska, on February 19, 2003 that could be related to that seismicity peak. Similarly, the seismicity peak on day 219 for the 2004 Banda Ache 6-month window (Figure 6, bottom) can be related to the M6.8 central Mid-Atlantic Ridge earthquake that occurred on January 12, 2005.

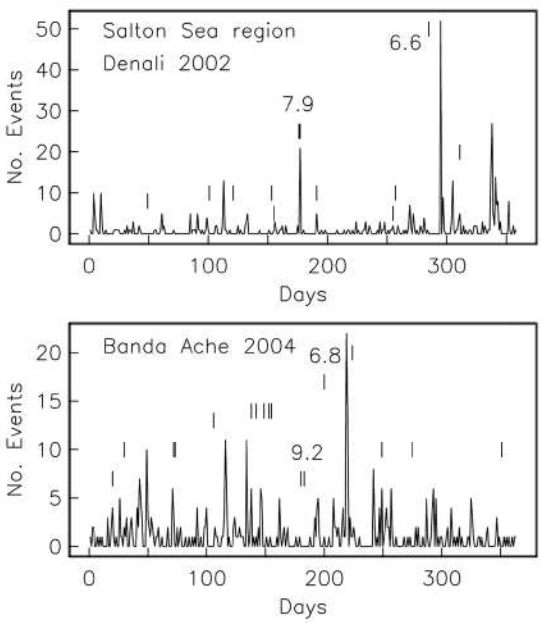

Figure 6. Number of events versus time in days for a 6-month period before and after the 2002 Denali fault (M7.9) earthquake (top frame) and for the 2004 Banda Ache, Sumatra (Mw9.2) earthquake (bottom frame). The vertical lines indicate the time of occurrence of big teleseismic (M>7.0) earthquakes.

The change in seismicity rate was quantified after the five mega-earthquakes by calculating the cumulative number of events in 60-day periods (Figure 7). The origin of the horizontal axis is the day of occurrence of the corresponding mega-event. The event rate variations seem to be randomly distributed before and after time zero. This observation suggests that different processes may be responsible for a swarm in geothermal fields. The β-statistics for the 30-day period was calculated after the five remote earthquakes for the Coso and Salton Sea regions, and for the total reference seismicity period of six months and 34 years (Table 1). The alternative Southern California catalog (Hauksson *et al*., 2012; Lin *et al*., 2007) was used for this calculation. The absolute values of β determined with equation (1) for the six month period are displayed in the lower right corner of each frame of Figure 7. In the Salton Sea region there is a clear change of seismicity rate on day zero, when the 2002 Denali fault earthquake occurred; 11 days after the 2004 Banda Ache event; 14 days after the 2010 Chile earthquake; 17 days after the 2011 Japan mega-quake; and 6 days after the 2012 Northern Sumatra earthquake.

As shown in Figures 4 and 5 most earthquakes had magnitudes below 2.0. Trugman *et al*. (2016) found that the minimum magnitude of completeness of the catalog increases during active earthquake sequences and swarms. Nevertheless, β was calculated using only events with magnitude above the conservative estimates of *Mc* obtained by Trugman *et al*. (2016), namely *Mc*=1.5 for Coso and *Mc*=2.0 for Salton Sea. Table 1 lists the present estimates of β for both regions for a 30-day period after the 5 teleseisms analyzed for the total reference periods of 60 days (30 days before and 30 days after the mega-earthquakes) and for a reference period of 34 years (the total period of the catalog). For the 60-day reference, in Salton Sea the change of seismicity rate is significant only after the Denali (M_w7.9) and the Chile (M_w8.8) earthquakes. For the Coso region the change is also significant after those events and after the Japan (M_w9.1) earthquake. For a total reference period of 34 years, the change of seismicity rate is significant after all the events in the Salton Sea region (Table 1). For the Coso region the change was not significant only for the Sumatra (Mw8.6).

The injection record of the geothermal fields (Figures 8 and 9) was plotted to verify that there were not significant changes of the injection parameters at the time when the seismicity rate-change takes place. No clear correlation

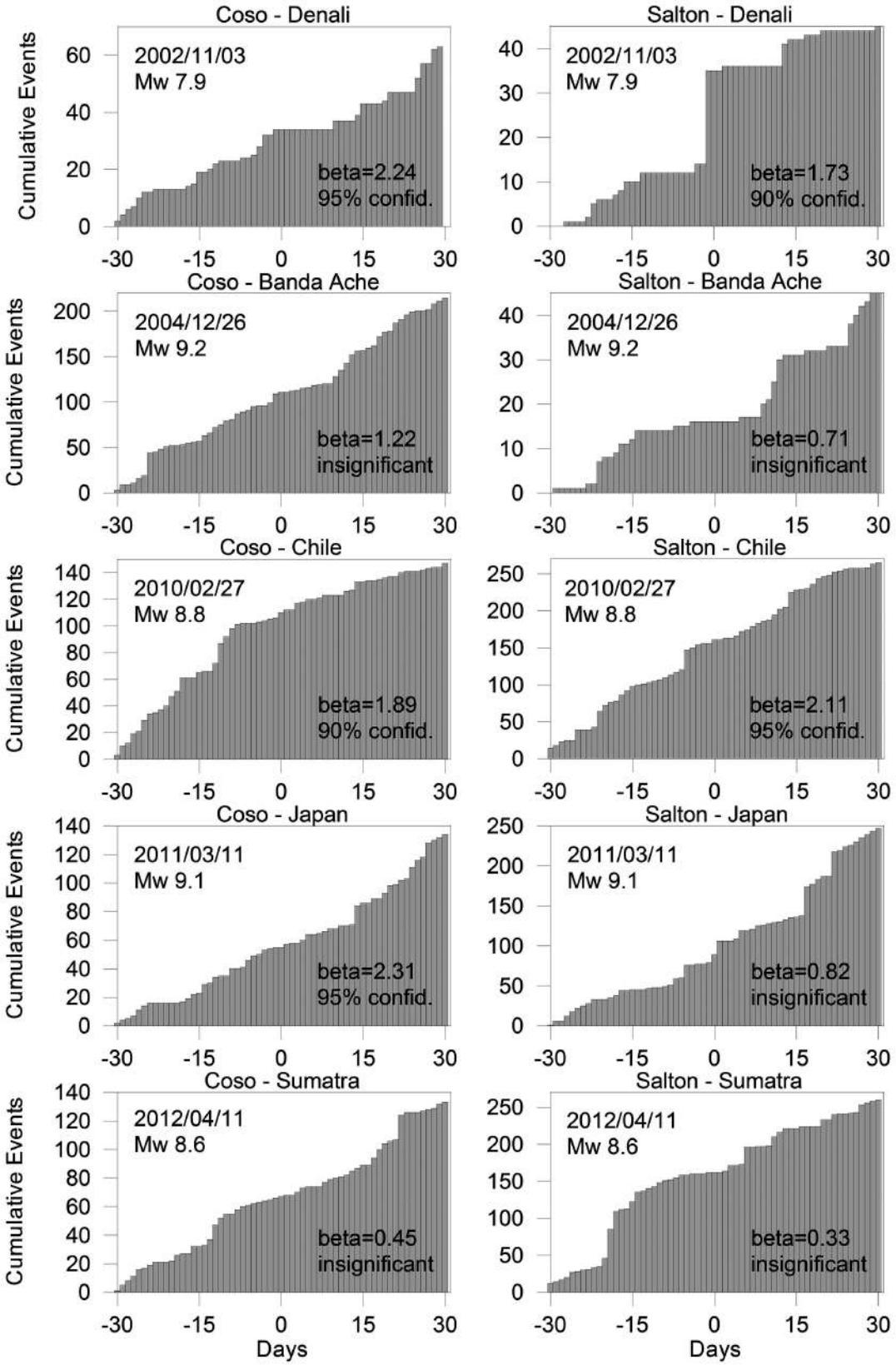

Figure 7. Cumulative number of events versus time for a 30-day period before and after the remote mega-earthquakes. Left column for the Coso region, right column for the Salton Sea region.

Table 1. Beta statistics for a 30-day period after the remote earthquake with respect to 60 days and 34 years of seismicity above Mc (the minimum magnitude of completeness for Coso and Salton Sea is 1.5 and 2.0, respectively).

EVENT	BETA (60 Days)	Confidence (%)	BETA (34 Yr)	Confidence (%)	REGION
Denali Mw7.9	1.73	90	6.1	99	Salton Sea
Banda Ache Mw9.2	0.71	Insignificant	3.6	99	
Chile Mw8.8	2.11	95	7.2	99	
Japan Mw9.1	0.82	Insignificant	11.9	99	
Sumatra Mw8.6	0.33	Insignificant	5.5	99	
Denali Mw7.9	2.24	95	3.7	99	Coso
Banda Ache Mw9.2	1.22	Insignificant	6.1	99	
Chile Mw8.8	1.89	90	2.7	99	
Japan Mw9.1	2.31	95	2.9	99	
Sumatra Mw8.6	0.45	Insignificant	1.2	Insignificant	

was observed between the seismicity rate-change and the net production (production minus injection) at neither geothermal field. Trugman *et al*. (2016) found that the seismicity rate in both fields correlates with fluid injection and withdrawal only before 1990, as shown in Figures 8 and 9.

Discussion

Different models have been proposed to explain delayed dynamic triggering of seismicity (Brodsky and Prejean, 2005; Parsons, 2005; Hill and Prejean, 2007; Shelly *et al*., 2011). The prolonged fault creep model (Shelly *et al*., 2011) proposes that large remote earthquakes can induce a creep event that may trigger earthquakes secondarily, with some time delay as creep evolves. If the passage of seismic waves generated by the mega-earthquakes analyzed changed the tectonic stress near the regions studied, when the size of the mega-event increases and/or the epicentral distance decreases, the dynamic stress is expected to increase. It may be also expected that the strength of the remote earthquake will be proportional to the size of the local events triggered. In Figure 10 (upper left) the maximum magnitude (M_{max}) of the delayed triggered earthquake swarm versus the seismic moment of the mega-earthquake divided by the epicentral distance (M_0/Δ) in dynes, is plotted. The solid line is the linear least-square fit of the observation points (asterisks and circles are observed data for Salton Sea and Coso, respectively) and indicates that the magnitude of the delayed trigged event increased with the size of the mega-earthquake. The resulting regression equation is:

$$Log\left(\frac{M_0}{\Delta}\right)=(19.35\pm0.40)+(0.44\pm0.17)\ M_{\max} \quad (2)$$

Figure 10 (upper right) also shows a positive correlation between the size of the mega-event and the delay time in days (D_t) and between D_t and the maximum magnitude of the triggered swarm (Figure 10 bottom). Based on the prolonged fault creep model (Shelly *et al*., 2011), it is expected that the duration of the creeping event may increase when the size of the remote earthquake increases. Thus, it would be expected that the delay time of the triggered events will increase. On the other hand, longer delay times permit greater accumulation of stress on the local faults and consequently larger magnitudes will be expected. The best least-square fit of these observations are represented by the following relations:

$$Log\left(\frac{M_0}{\Delta}\right)=(19.79\pm0.28)+(0.44\pm0.02)\ D_{\mathrm{t}} \quad (3)$$

$$M_{max}=(1.58\pm0.54)+(0.056\pm0.04)\ Dt \quad (4)$$

Making M_0/Δ the independent variable, the resulting regressions give:

$$M_{max}=(-22.53\pm9.41)+(1.21\pm0.46)Log\left(\frac{M_0}{\Delta}\right) \quad (5)$$

$$D_t=(-211.8\pm94.6)+(11.06\pm4.64)Log\left(\frac{M_0}{\Delta}\right) \quad (6)$$

Equations (5) and (6) predict that for an earthquake like Japan 2011 having $\frac{M_0}{\Delta}$ =0.6435x10^{21} dynes, the maximum magnitude expected for a local event triggered in Salton Sea or Cosco regions will be M_{max}=2.6 and will occur seven days after the remote earthquake.

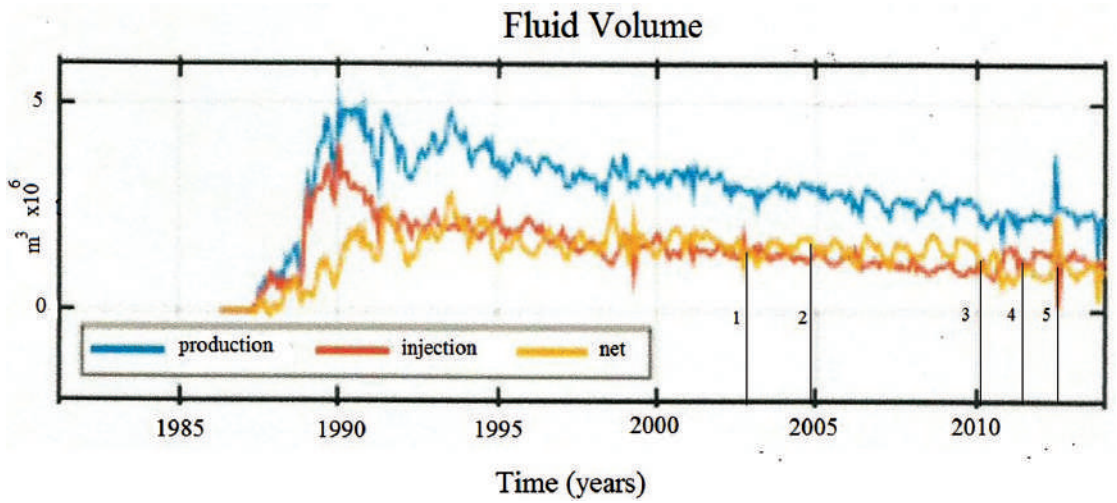

Figure 8. Monthly rate fluid injection (red), production (blue), and net production (yellow) (modified from Trugman *et al*., 2016) at Coso geothermal field (data available at http://www.conservation.ca.gov/dog/geothermal). The vertical lines (black) indicate the date when the remote earthquakes occurred: (1) the November, 2002 Denali fault, Alaska (*Mw*7.9); (2) the December, 2004 Banda Ache (*Mw*9.2); (3) the February, 2010 Central Chile (*Mw*8.8); (4) the March, 2011 Tohoku-Oki, Japan (*Mw*9.1); (5) the April, 2012 Northern Sumatra (*Mw*8.6) earthquake.

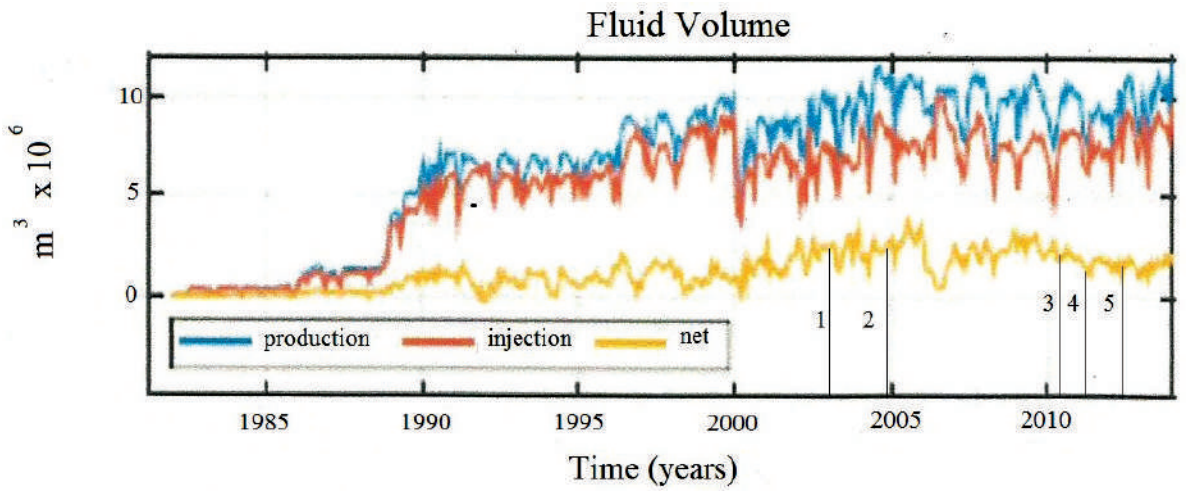

Figure 9. Same as in Figure 8 but for Salton Sea geothermal field.

Other regions may be able to generate bigger magnitude events. For instance, Gonzalez-Huizar *et al*. (2012) observed delayed triggering of larger magnitudes, including an *M*=5.2, in the southern Gulf of California following the 2011 Tohoku-Oki earthquake. Equations (5) and (6) should be used with caution because the data set used to obtain them is small and spread. However, these equations permit to quantify the trends of the observations here presented.

An alternative model to explain the delayed triggered seismicity and the spatial distribution pattern of earthquakes observed in Figures 2 and 3 is to consider that the surface waves generated by the large distant events induce the migration of pressurized pore fluids (e.g. Malagnini *et al*., 2012). The migration of fluids can cause an increase in pore pressure and the decrease in shear strength on the fault planes, inducing earthquakes. This diffusion-like process can be modeled as a 1-D steady state source of pressure that starts when the

Rayleigh wave reach the region of interest. The solution to this 1-D diffusion process is given by Turcotte and Schubert (1982):

$$P(x,t) = (P_0\text{-}P_1)\,erfc\left(\frac{x}{2\sqrt{Dt}}\right) + P_1 \quad (7)$$

With the following boundary and initial conditions:

$$P(x = 0,\, t > 0) = P_0 = \gamma_f \rho_r g z \quad (8)$$

$$P(x > 0,\, t = 0) = P_1 = \rho_w g z \quad (9)$$

Where *erfc* is the complementary error function, *D* is the diffusion coefficient, γ_f = 0.8 is the pore fluid coefficient, ρ_r = 2.99 gr/cm^3, *z* = 3 km is the depth and ρ_w is the density of the water. Turcotte and Schubert (1982) show that the position of the pressure boundary can be estimated with the relation:

$$x_p = 2.32\sqrt{Dt} \quad (10)$$

This model was tested with the seismicity triggered by the 2011 Japan (M_w9.1) earthquake (fourth row of Figures 4 and 5). This earthquake was selected because it is one of the biggest and it triggered delayed and instantaneous seismicity in both Coso and Salton Sea geothermal fields. The fluid flow was assumed to start with the arrival of the Rayleigh waves generated by the Japan earthquake to the geothermal fields and that the seismicity migrates in the same direction of the pressure boundary following equation (10). The first event triggered with the Rayleigh wave arrival was used as a reference origin and relative distances were calculated. Figure 11 shows time of occurrence in days versus relative distance in km. The solid lines are the expected position of the pressure boundary for different values of the diffusion coefficient D. This figure illustrates that the seismicity in

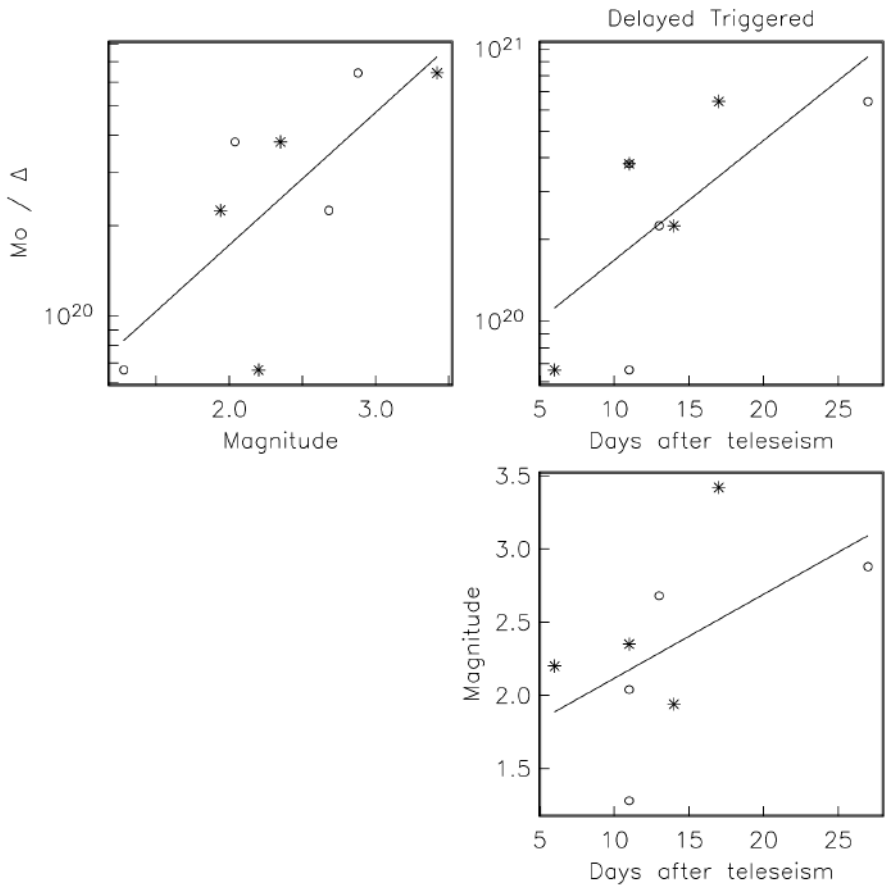

Figure 10. Correlation between size of remote earthquakes (seismic moment/epicentral distance) and maximum magnitude of the triggered event (upper left frame) in the Salton Sea (asterisks) and in the Coso Range (circles) regions. The upper right shows the time delay in days after the mega-earthquake. The bottom frame shows the relation between time after the mega-earthquake and the maximum magnitude of the local event triggered.

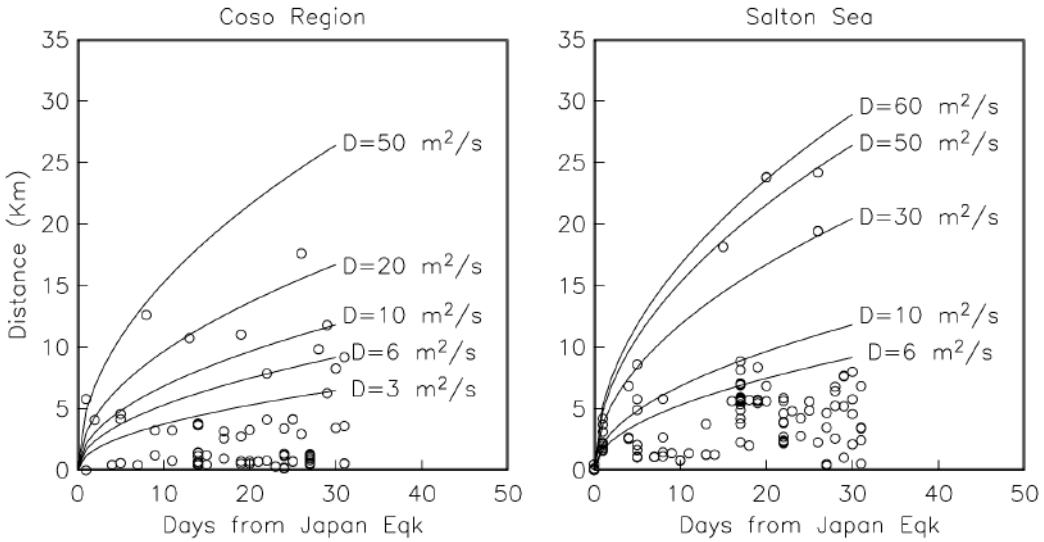

Figure 11. Events that occurred 30 days after the 2011 Japan (M_w9.1) earthquake in the Coso region (left) and in the Salton Sea region (right). The distance is relative to the first event of the swarm that occurred after the Japan earthquake. The solid lines are the expected position of the pressure boundary for different values of the diffusion coefficient D (equation 10).

the 30-day window after the Japan earthquake seems to follow a diffuse pattern, as predicted by the 1-D model (equations 7 and 10). The Rayleigh waves propagate toward the SE and seismicity is expected to migrate in the same direction. In the Salton Sea region, for instance, events with larger relative distance (Figure 9 right) are located south of the geothermal field (Figure 3d).

Conclusions

The 2011-Hauksson-Yang-Shearer alternative catalog of Southern California was used to analyze possible changes in seismicity rate in the Coso and Salton Sea, southern California, during and after five large (M_W>7.8) and remote earthquakes. The 2002 Denali fault (M_W7.9) earthquake and the 2011 Tohoku-Oki (M_W9.1) earthquake generated an increase of seismicity in the Salton Sea region the day when these remote events occurred, indicating that instantaneous triggered seismicity was likely induced by the passage of the surface waves. No instantaneous triggering was detected in the Coso region with the alternative seismicity catalog of southern California but a clear delayed triggered seismicity was observed after the Mw7.9 Denali, the Mw8.8 Chile and the M_w9.1 Japan. Delayed triggered seismicity in the Salton Sea for those earthquakes was also observed.

In conclusion the observations of delayed triggering presented here are consistent with the prolonged fault creep model proposed by Shelly *et al*. (2011). The stronger the dynamic stress the bigger the creeping event induced and the longer the delay of the triggered event. Equation (4) indicates that the longer the delay time the bigger the maximum magnitude of the expected triggered earthquake. The resulting regressions (equations 5 and 6) could be useful to evaluate if remote mega-earthquakes can trigger significant size earthquakes locally, and when the triggered seismicity could occur. However, this process also depends on the earthquake cycle of the active region and those regressions should be used with caution until more data is available to verify the observed trends. The spatial-temporal distribution of the seismicity in Coso and Salton Sea geothermal fields following the 2011 Japan earthquake is also consistent with a diffusion model where migration of fluids can cause increase in pore pressure and the decrease in shear strength that induces earthquakes. This alternative model to explain the delayed triggered seismicity and the spatial distribution pattern of earthquakes observed is complex because it relies on the wave propagation characteristics of the Rayleigh waves.

Acknowledgements

This paper was prepared while the first author (RRC) was on sabbatical year in Caltech. We thank CONACYT and Prof. Gurnis for the support provided. Antonio Mendoza helped us to prepare some maps. We used parametric data from the Caltech/USGS Southern California Seismic Network (SCSN); DOI: 10.7914/SN/CI; stored at the Southern California Earthquake Center. doi:10.7909/C3WD3xH1. We thank the two anonymous reviewers and the Editor Dr. Xyoli Pérez-Campos for their comments and suggestions.

References

Aiken C., Peng Z., 2014, Dynamic triggering of microearthquakes in three geothermal/volcanic regions of California. *J. Geophys. Res. Solid Earth*, 119, 6992-7009.

Anderson J.G., Brune J.N., Lowie J.N., Zeng Y., Savage M., Yu G., Chen Q., dePolo D., 1994, Seismicity in the western Great Basin apparently triggered by the Landers, California, earthquake, 28 June 1992. *Bull. Seism. Soc. Am.*, 84, 863-891.

Aron A., Hardebeck J.L., 2009, Seismicity rate changes along the central California coast due to stress changes from the 2003 M6.5 San Simeon and 2004 M6.0 Parkfield earthquakes. *Bull. Seism. Soc. Am.*, 99, 2280-2292.

Barak S., Klemperer S.L., Lawrence J.F., 2015, San Andreas fault dip, Peninsular Ranges mafic lower crust and partial melt in the Salton Trough, Southern California, from ambient-noise tomography, Geoch., Geophys., *Geosystems*, *AGU Publications*, doi:10.1002/2015GC005970.

Bhattacharyya J., Lees J.M., 2002, Seismicity and seismic stress in the Coso Range, Coso geothermal field, and Indian Wells Valley region, southeast-central California, Mem. *Geol. Soc. Am*., 195, 243-257.

Brodsky E.E., Prejean S.G., 2005, New constraints on mechanisms of remotely triggered seismicity at Long Valley Caldera. *J. Geophys. Res*., 110, B04302, doi:10.1029/2004JB003211.

Brodsky E.E., Lajoie L.J., 2013, Anthropogenic seismicity rates and operational parameters at the Salton Sea Geothermal Field, *Science*, 341, 543-546, doi:10.1785/0220150004.

Castro R.R., González-Huízar H., Zúñiga F.R., Wong V.M., Velasco A.A., 2015, Delayed dynamic triggered seismicity in northern Baja California, Mexico caused by large and remote earthquakes, *Bull. Seism. Soc. Am*., 105, 1825-1835.

Doran A.K., Peng Z., Meng X., Wu C., Kilb D., 2011, Dynamic triggering of earthquakes in the Salton Trough of southern California, *Seismol. Res. Lett*., 82, 2.

Doser D.I., Kanamori H., 1986, Depth of seismicity in the Imperial Valley region (1977-1983) and its relationship to heat flow, crustal structure and the October 15, 1979, eqrthquake, *J. Geophys. Res.*, 91, 675-688.

Eberhart-Phillips D., Haeussler P.J., Freymueller J.T., Frankel A.D., Rubin C.M., Craw P., Ratchkovski N.A., Anderson G., Carver G.A., Crone A.J., Dawson T.E., Fletcher H., Hansen R., Harp E.L., Harris R.A., Hill D.P., Hreinsdóttir S., Jibson R.W., Jones L.M., Kayen R., Keefer D.K., Larsen C.F., Moran S.C., Personius S.F., Plafker G., Sherrod B., Sieh K., Sitar N., Wallace W.K., 2003, The 2002 Denali fault earthquake, Alaska: A large magnitude, slip-partitioned event, *Science*, 300, 1113-1118, doi:10.1126/science.1082703.

Elders W.A., Rex R.W., Robinson P.T., Biehler S., Meidav T., 1972, Crustal spreading in southern California: The Imperial Valley and the Gulf of California formed by the rifting apart of a continental plate, *Science*, 178, 15-24.

Feng Q., Lees J.M., 1998, Microseismicity, stress and fracture in the Coso Geothermal Field, California, *Tectonophys.*, 289, 221-238, doi:10.1016/S0040-1951(97)00317-X.

Fuis G.S., Mooney W.D., Healy J.H., McMechan G.A., Lutter W.J., 1984, A seismic refraction survey of the Imperial Valley region, California, *J. Geophys. Res.*, 89, 1165-1189.

Gomberg J., Bodin P., 1994, Triggering of the Ms=5.4 Little Skull Mountain, Nevada, earthquake with dynamic strains, *Bull. Seism. Soc. Am.*, 84, 844-853.

Gomberg J., Bodin P., Larson K., Dragert H., 2004, Earthquake nucleation by transient deformations caused by the M=7.9 Denali, Alaska, earthquake, *Nature*, 427, 621-624, doi:10.1038/nature02335.

Gonzalez-Huizar, Velasco, 2011, Dynamic triggering: Stress modeling and a case study, *J. Geophys. Res*., 116, B02304, doi:10.1029/2009JB007000.

Gonzalez-Huizar, H., A.A. Velasco, Z. Peng, and R. Castro (2012). Remote triggered seismicity caused by the 2011, M9.0 Tohoku-Oki, Japan earthquake, *Geophys. Res. Lett*., 39, L10302, doi:10.1029/2012GL051015,2012.

Hauksson, E., K. Hutton, H. Kanamori, L. Jones, J. Mori, S. Hough, and G. Roquemore (1995). Preliminary report on the 1995 Ridgecrest earthquake sequence in eastern California, *Seismol. Res. Lett.*, 66, 54-60.

Hauksson, E., and J. Unruh (2007). Regional tectonics of the Coso geothermal area along the intracontinental plate boundary in central eastern California: Three-dimensional Vp and Vp/Vs models, spatial-temporal seismicity patterns, and seismogenic deformation. *J. Geophys. Res.*, 112, B06309, doi:10.1029/2006JB004721.

Hauksson, E. (2011). Crustal geophysics and seismicity in southern California, *Geophys. J. Int.*, 186, 82-98.

Hauksson, E., W. Yang, and P.M. Shearer (2012). Wave form relocated earthquake catalog for Southern California (1981 to 2011). *Bull. Seism. Soc. Am*., 102, 2239-2244.

Hill, D.P., P.A. Reasenberg, A. Michael, W.J., Arabaz, G. Beroza, D. Brumbough, J.N., Brune, R. Castro., S. Davis, D. de Polo, W.L. Ellsworth, J. Gomberg, S. Harmson, L. House, S.M. Jackson, M.J.S. Johnston, L. Jones, R. Keller, S. Malone, L. Munguía, S. Nava, J.C. Pechmann, A. Sanford, R.W. Simpson,R.B. Smith, M. Stark, M. Stickney, A. Vidal, S. Walter, V. Wong, J. Zollweg (1993). Seismicity remotely triggered by the Magnitude 7.3 Landers, California, Earthquake, *Science*, 260, 1617-1623.

Hill, D. P., and S. G. Prejean (2007). Dynamic triggering, in Treatise on Geophysics, 257–292, ed. Schubert, G., Vol. 4: Earthquake Seismology, ed. Kanamori, H., Elsevier, Amsterdam.

Hill, D.P. (2008). Dynamic stresses, coulomb failure, and remote triggering, *Bull. Seism. Soc. Am.*, 98, 66-92.

Hough, S.E., and H. Kanamori (2002). Source properties of earthquakes near Salton Sea triggered by the 16 October 1999 *M*7.1 Hector Mine, California, earthquake, *Bull. Seismol. Soc. Am*., 92, 1281-1289.

Hough, S.E. (2007). Remotely triggered earthquakes following moderate main shocks, Spec. Pap. Geol. Soc. Am., 425, 73-86.

Hubbert, M.K., and W.W. Rubey (1959). Role of fluid pressure in mechanics of overthrust faulting, *Geol. Soc. Am. Bull*., 70, 115-166.

International Seismological Centre, On-line Bulletin, http://www.isc.ac.uk, Internatl. Seis. Cent. Thatcham, United Kingdom, 2016.

Jiang, T., Z. Peng, W. Wang, and Q.-F. Chen (2010). Remotely triggered seismicity in continental China by the 2008 Mw7.9 Wenchuan earthquake, *Bull. Seismol. Soc. Am*., 100, 2574-2589, doi:10.1785/0120090286.

Lachenbruch, A.H.A., J.H. Sass, S.P. Galanis, and S. Galanis Jr. (1985). Heat flow in southernmost California and the origin of the Salton Trough, *J. Geophys. Res*., 90, 6709-6736.

Lin, G., P.M. Shearer, and E. Hauksson (2007). Applying a three-dimensional velocity model, wave form cross correlation, and cluster analysis to locate southern California seismicity from 1981 to 2005. *J. Geophys. Res.*, 112, B12309, doi:10.1029/2007JB004986.

Linde, A.T., and I.S. Sacks (1998). Triggering of volcanic eruptions, *Nature*, 395, 888-890.

Malagnini, L., F.P. Lucente, P. De Gori, A. Akinci, and I. Munafo (2012). Control of pore fluid pressure diffusion on fault failure mode: Insights from the 2009 L'Aquila seismic sequence. *J. Geophys. Res*., 117, B05302, DOI:10.1029/2011JB008911.

Matthews, M.V., and P.A. Reasenberg (1988). Statistical methods for investigating quiescence and other temporal seismicity patterns. *Pure Appl. Geophys*., 126, 357-372.

Monastero, F.C., A.M., Katzenstein, J.S., Miller, J.R., Unruh, M.C., Adams, K., Richards-Dinger (2005). The Coso geothermal field: A nascent metamorphic core complex. *GSA Bulletin*, 117, 1534-1553, DOI:10.1130/B25600.1

Muffler, L.J., and D.E. White (1969). Active metamorphism of upper Cenozoic sediments in the Salton Sea Geothermal Field and the Salton Trough, Southeastern California, *Geol. Soc. Am. Bull*., 80, 157-182.

Pankow K.L., Arabasz W.J., Pechmann J.C., Nava S.J., 2004, Triggered seismicity in Utah from the November 3, 2002, Denali fault earthquake, *Bull. Seismol. Soc. Am.*, 94, S332-S347.

Parsons T., 2005, A hypothesis for delayed dynamic earthquake triggering, *Geophys. Res. Lett*. 32, L04302, doi: 10.1029/2004GL021811

Peng Z., Gomberg J., 2010, An integrated perspective of the continuum between earthquakes and slow-slip phenomena, *Nat. Geosci*., 3, 599-607, doi:10.1038/ngeo940.

Peng Z., Hill D.P., Shelly D.R., Aiken C., 2010, Remotely triggered microearthquakes and tremor in central California following the 2010 Mw 8.8 Chile earthquake. *Geophys. Res. Lett.*, 37, L24312, doi:10.1029/2010GL045462

Peng Z., Wu C., Aiken C., 2011, Delayed triggering of microearthquakes by multiple surface waves circling the Earth. *Geophys. Res. Lett*., 38, L04306, doi:10.1029/2010GL046373.

Pollitz F.F., Stein R.S., Sevilgen V., Burgmann R., 2012, The 11 April 2012 east Indian Ocean earthquake triggered large aftershock worldwide, *Nature*, 490, doi:10.1038/nature11504

Prejean S.G., Hill D.P., Brodsky E.E., Hough S.E., Johnson M.J.S., Malone S.D., Oppenheimer D.H., Pitt A.M., Richards-Dinger K.B., 2004, Remotely triggered seismicity on the United States west coast following the M 7.9 Denali fault earthquake, *Bull. Seismol. Soc. Am*., 94, S348-S359.

Ryan W.B.F., Carbotte S.M., Coplan J.O., O'Hara S., Melkonian A., Arko R., Weissel R.A., Ferrini V., Goodwillie A., Nitsche F., Bonczkowski J., Zemsky R., 2009, Global Multi-Resolution Topography synthesis, Geochem. *Geophys. Geosys*., 10, Q03014, DOI:10.1029/2008GC002332.

Schmitt A.K., Martin A., Stockli D.F., Farley K.A., Lovera O.M., 2013, (U-Th)/He zircon and archaeological ages for a late prehistoric eruption in the Salton Trough (California,USA), *Geology*, 41, 7-10.

Shelly D.R., Peng Z., Hill D., Aiken C., 2011, Triggered creep as a possible mechanism for delayed dynamic triggering of tremor and earthquakes, *Nature Geosci.,* 4, 384-388.

Stock J.M., Hodges K.V., 1989, Pre-Pliocene extension around the Gulf of California and the transfer of Baja California to the Pacific Plate, *Tectonics*, 8, 99-115.

Trugman D., Shearer P.M., Borsa A.A., Fialko Y., 2016, A comparison of long-term changes in seismicity at the Geysers, Salton Sea, and Coso geothermal fields, *J. Geophys. Res. Solid Earth*, 121, 225-247, doi:10.1002/2015JB012510.

Turcotte D.L., Schubert G., 1982, Geodynamics: Applications of continuum Physics to geological problems, 450 pp., John Wiley, New York.

West M., Sanchez J.J., McNutt S.R., 2005, Periodically triggered seismicity at Mount Wrangell, Alaska, after the Sumatra earthquake, *Science*, 308, 1144-1146, doi:10.1126/science.1112462.

Velasco A.A., Hernandez S., Parsons T., Parkow K., 2008, Global ubiquity of dynamic earthquake triggering, *Nat. Geosci*., 1, 375-379, doi:10.1038/ngeo204.